MACROMIXING STUDY FOR VARIOUS DESIGNS OF IMPELLERS IN A STIRRED VESSEL

Reza Afshar Ghotli[a,*], Mohammad Saleh Shafeeyan[b], Mohammad Reza Abbasi[c], Abdul Raman Abdul Aziz[d], Shaliza Ibrahim[a]

[a]Reza Afshar Ghotli (Corresponding author)

Institute of Ocean and Earth Sciences (IOES), Research Management and Innovation Centre, University of Malaya, 50603 Kuala Lumpur, Malaysia

E-mail: afsharghotli_reza@yahoo.com

[b]Mohammad Saleh Shafeeyan

Department of Chemical Engineering, Faculty of Engineering, Golestan University, Aliabad Katoul, Iran

E-mail: ms.shafeeyan@gu.ac.ir

[c]Mohammad Reza Abbasi

Department of Chemical Engineering, University College London (UCL), Torrington Place, London WC1E 7JE United Kingdom

E-mail: r.abbasi@ucl.ac.uk

[d]Abdul Aziz Abdul Raman

Department of Chemical Engineering, Faculty of Engineering, University of Malaya, 50603, Kuala Lumpur, Malaysia

E-mail: azizraman@um.edu.my

[a]Shaliza Ibrahim

 Institute of Ocean and Earth Sciences (IOES), Research Management and Innovation Centre, University of Malaya, 50603 Kuala Lumpur, Malaysia

E-mail: shaliza@um.edu.my

Abstract

The effect of the impeller designs and impeller clearance level (C/T) on power consumption, mixing time and air entrainment point in a single liquid phase under turbulent conditions (Re>10^4) were investigated. Different impeller designs including conventional and new designs, were used to consider both axial and radial flow impellers. The electric conductivity method, suspended motor system and observation method were employed to determine the mixing time, the power consumption and the air entrainment point, respectively. The reduction in the impeller clearance level form T/3 to T/6 resulted in a decrease in power number values for up-flow pumping impellers while it was increased for down-flow pumping. The same trend was observed for the mixing time results. Moreover, axial flow impellers and specially HE3 are preferable for higher agitation speeds due to the less air entrainment. The results verified that the axial flow impellers and specifically down-flow impellers are more efficient than the radial flow impellers. ANFIS-Fuzzy C–means (ANFIS–FcM) and nonlinear regression were used to develop models to predict the mixing time based on the energy dissipation rate and clearance. The results verified that the model predictions successfully fit the experimental mixing time data.

Keywords: Impeller design, Clearance level; Energy dissipation rate; Mixing time; Nonlinear regression; ANFIS-Fuzzy C-means

1 Introduction

Mechanical agitation is widely employed in chemical process industries for heat and mass transfer applications or chemical reactions applications [1]. Precipitation, polymerization and hydrometallurgical processes are usually conducted using mechanical agitation. The efficiency of the mixing process is dependent on different internal parameters such as agitation speed, impeller type, tank geometry, geometrical ratios such as impeller to tank diameter (D/T), off-bottom clearance to tank diameter (C/T), liquid height to tank diameter (H/D), dispersed phase hold-up and fluid physical properties. Therefore, any small changes in vessel and impeller geometries has considerable effects on the power consumption, flow pattern, drop size distribution, mixing time and consequently on the mixing characteristics [2, 3]. In last 60 years, several impellers have been designed and developed for better efficiency in various applications but Rushton turbine, pitched blade turbines and propellers were the most common employed impellers [4-10].

Power consumption and mixing time are two parameters with a significant role in evaluating the performance of stirred vessels. Power consumption is defined as the required amount of energy per unit of time and mixing time is understood as the time required to obtain a certain degree of uniformity in a stirred vessel [3]. The stirred vessel configuration has a direct effect on these parameters and consequent influence on operating cost and product quality [1, 9, 11, 12]. Thus, the comparison of these parameters for various impeller designs and impeller off-bottom clearance level gives valuable information about the performance of the agitation systems [1, 13]. Furthermore, it is also helpful to improve and develop the design of reactors especially when the geometrical design and the condition of experiments are comparable. However, achievement of desired level of mixing is expected at the lowest value of the power consumption [5].

1   Several studies have been accomplished on the effect of impeller designs and configurations

2   on mixing parameters. Raghav Rao and Joshi [14] performed extensive experiments to study the

3   effect of clearance for different design of impellers on the power consumption per unit volume of

4   liquid and pointed out better efficiency for down- flow pitched blade turbine. They reported a

5   reduction in mixing time with decreasing the clearance for disk turbine and pitched blade up-

6   flow turbine while it was increased in the case of pitched-blade down-flow turbine. Rewatkar

7   and Joshi [14] also studied the effect of impeller clearances and impeller designs on mixing

8   times. They reported that the pitched blade turbine both down- flow and up-flow are more energy

9   efficient than the disk turbine design at equal power consumption per mass. They also stated the

10   same dimensionless mixing time for all of these impellers. The variety in relative performance

11   was due to the different values of impeller power number. They also indicated a decrease in

12   mixing time with increasing the blade angle for pitched blade turbines and the PBTD45 was the

13   most efficient one. Further increase was observed for mixing time with decreasing the impeller

14   diameter [5]. Rzyski [15] reported lowest mixing time for propeller among a six blade disk

15   turbine (DT), propeller (with two different pitches), and six-blade fan-type turbine at equal

16   power consumption. The results verified that the performance of axial flow impellers is close

17   together and their mixing time is lower than radial flow turbines. Ruszkowski [16] found the

18   same mixing time was observed for pitched blade turbines with different blade numbers and

19   blade angles, six blade DT and propeller at equal power consumption. Moreover, a large

20   diameter with low power number was suggested as the most energy efficient one in turbulent

21   mixing. Distelhoff et al. [17] reported the same results with Raghav Rao and Josi [14] and

22   Rewatkar and Joshi [5] with lower mixing times for the down-flow pitched blade turbine than the

23   radial flow impeller. Houcine et al. [1] also reported an increase in mixing time values with

1   decreasing the clearance from T/2 to T/3 for pitched blade turbine while decreasing for Rushton

2   turbine and MIXEL propellers.

3   Nere et al. [2] performed extensive experiments to examine the effect of different impeller

4   and tank geometries on the mixing times. They stated that the dimensionless mixing time

5   changes reversely with the cube root of the power consumed per unit volume of the liquid. The

6   constant was obtained at 7.9 for the disk turbine while it was 4.38 for the propeller. The results

7   were inconsistent with the outcomes presented by kramers et al. [4]. They notified that the

8   clearance level is dependent to the impeller designs and tank geometries. They recommended to

9   use C/T=1/3 in the case of PBTD, DT and marine propeller inline to other previous studies [2].

10 Kumaresan and Jushi [7] found that, irrespective of the impeller design, the mixing time was to

11 be inversely proportional to the secondary flow number (N_{QS}) for 18 different designs of

12 impellers including PBT, Hydrofoil impellers and Rushton turbine with variances in blade angle,

13 number of blades, blade width, blade twist, and blade thickness through LDA measurement.

14 They indicated 3% less power number and 7% reduction in average normal stress at the higher

15 clearance level for PBTD turbine which resulted in higher mixing time [7]. Aubin et al. [18]

16 obtained that the axial up-pumping flow impellers reduce the mixing time and increase

17 turbulence in batch reactors through CFD modeling. Ochieng and Onyango [12] showed that the

18 flow pattern for the Rushton turbine changed from the typical two loops to a single loop similar

19 to axial flow impellers at the low off-bottom clearance which was caused in a lower mixing time

20 at a constant power number`. Woziwodzki [19] achieved higher mixing time in an un-baffled

21 vessel compared to the baffled vessel for turbine impeller. Afshar Ghotli et al. [20] investigated

22 various curved blade impellers and indicated higher power number for wider curvature blades.

1 Moreover, lower power consumption was observed for the curved blade impellers compared

2 with the Rushton turbine.

3 Several correlations have been developed to predict the mixing time within the stirred

4 vessels to estimate the mixing efficiency. Some of these correlations were derived based on the

5 dimensionless mixing time. Dimensionless mixing time (Nt_m) is depended on the impeller and

6 tank geometries in turbulent condition [21]. However, most of the correlations have been

7 developed based on the mixing time. The effect of Froude number and Reynolds number can be

8 neglected under the turbulent condition. Prochazka and Landau [22] developed correlations to

9 estimate the mixing time for Rushton turbine, propeller and pitched blade, separately, for a

10 standard stirred vessel under turbulent conditions [23]. One of the best correlations between the

11 mixing time and power consumption per unit volume was suggested by Moo-Young et al. [24]

12 and Nienow [25]:

13 $$t_m = c(\bar{\varepsilon}_T)^d \tag{1}$$

14 The value of "d" was found approximately – 0.33 for turbulent regime in many studies. The

15 value of "c" can be determined experimentally, and it is depended on the impeller and vessel

16 geometry. Pakzad et al. [26] reported the value of "*c*" and "*d*" at 113.3 and −0.33 for transient

17 regime, respectively. Woziwodzki [19] found the value of 3.9 for the "*c*". Van riet and Tramper

18 [27] derived a theoretical correlation [25]:

19 $$t_m N = 3\left(\frac{D}{T}\right)^{-3} N_P^{-1/3} \tag{2}$$

20 Ruszkowski [16] and Grenville et al. [28] developed correlation (3) to estimate the mixing time

21 for various impeller geometries at H=T and energy dissipation rates of 1 W/kg [29]

22 $$t_m = c\left(\frac{1}{N}\right)\left(\frac{1}{N_P^{1/3}}\right)\left(\frac{D}{T}\right)^{-2} \tag{3}$$

1   The value of "A" was defined by Ruszkowski [16], Grenville et al. [28] at 0.53. Thus;

2     $$t_m = 5.9 T^{2/3} \left(\bar{\varepsilon}_T \right)^{-1/3} \left(\frac{D}{T} \right)^{-1/3}$$ (4)

3   A good agreement was found for this equation with different impellers with different ratio of

4   D/T [25, 30-32].

5   Pandit and Joshi [33] developed the equations to estimate mixing time on the basis of flow

6   pattern for DT, PTD and PTU, respectively [14]:

7     $$t_m = 9.43 \left(\frac{1}{N} \right) \left(\frac{aH+T}{T} \right) \left(\frac{T}{D} \right)^{13/6} \left(\frac{W}{D} \right)$$ (5)

8     $$t_m = 5.0 \left(\frac{1}{N} \right) \left(\frac{2H}{D} + \frac{T}{D} \right) \left(\frac{C}{D} \right)$$ (6)

9     $$t_m = 5.0 \left(\frac{1}{N} \right) \left(\frac{2H}{D} + \frac{T}{D} \right) \left(\frac{H-C}{D} \right)$$ (7)

10   Rewatkar and Joshi [5] developed a correlation for pitched blade turbine to show the effect of

11   impeller blade angle (A), a ratio of blade width to impeller diameter (W/D), number of blades

12   (n_b), a ratio of tank diameter to impeller diameter (T/D), a ratio of impeller clearance to tank

13   diameter (C/T) and a ratio of liquid height to tank diameter (H/T) on mixing time.

14     $$t_m = 5.37 \left(\frac{1}{N} \right) (\text{A})^{-0.87} \left(\frac{W}{D} \right)^{-0.314} (n_b)^{-0.482} \left(\frac{T}{D} \right)^{1.83} \left(\frac{C}{T} \right)^{-0.27} \left(\frac{H}{T} \right)^{0.413}$$ (8)

15   Though, several studies on the effect of impeller design on mixing efficiency can be found

16   through the literature, few of them considered a wide range of impeller designs. Accordingly, the

17   purpose of this effort is to provide the macromixing reports for different impeller designs. The

18   effect of impeller types, impeller clearance and agitation speed on mixing time, power

19   consumption and air entrainment point has been studied. Various design of impellers namely

1   Rushton turbine (RT), up-flow pitched-blade turbine (PBTU), down-flow pitched-blade turbine

2   (PBTD), semicircular blade (CB), parabolic blade (PB), axial flow hydrofoil impeller (HE3) and

3   newly designed double circular blade (DCB) have been employed. The present work aims to

4   evaluate the efficiency of various impellers at different clearance levels with regard to the

5   variation of the power consumptions and mixing times for turbulent system (Re $>10^4$). In

6   addition to the experimental study, the purpose of this work is to provide accurate models to

7   predict the mixing time based on attributes of different impeller designs off-bottom clearance.

8   Therefore, non-linear regression method and adaptive neuro-fuzzy inference system, based on

9   fuzzy c–means clustering algorithm (ANFIS–FcM) were applied in order to determine the

10   relationships between input and output parameters. These methods are followed to develop

11   accurate models to predict the mixing time and to discuss the results.

12   **2   Materials and Experimental setup**

13   **2.1   Set up**

14   A flat-bottomed agitated vessel with a volume of 0.022 m^3 (22 L) and an internal diameter

15   of 0.3 m were used for all the measurements. Four removable wall mounted baffles were fitted

16   equally spaced. Different designs of impellers including Rushton turbine (RT), 45° up-flow

17   pitched blade turbine (PBTU), 45° down-flow pitched blade turbine (PTBD), semi-circular blade

18   (CB), parabolic blade (PB), hydrofoil (HE3) and newly designed double circular blade (DCB)

19   impellers, were employed. The hydrofoil design is disclosed in European Patent EP 0 465 636

20   B1. Fig. 1 and Fig. 2 illustrate the schematic of experimental setup and impeller designs,

21   respectively. The pitched blade turbines hydrofoil impeller are belonging to the axial flow

22   impellers. These impellers provide suction and pumping in a direction parallel to the shaft axis

23   [34]. The hydrofoil impeller is designed in 3-bladed impeller while the pitched blade turbines

1 have 6-blade with 45° angle. Besides, the Rushton turbine, semi-circular blade, double circular

2 blade, parabolic blades are radial flow impellers. The suction flow is in a direction parallel to the

3 shaft axis while pumping is normal to the shaft [34]. All of the radial impellers are provided in

4 six-bladed designs. The ratio of impeller diameter to the tank diameter is equal to 1/3 for all of

5 the impellers. The ratio of impeller clearance (C) to the tank diameter (T) set at T/3, T/4 and T/6.

6 The rotational speed is varied in a range of 1.67 rps to 15 rps to provide the turbulent flow

7 regime. The vessel was filled with distilled water as a working fluid and the liquid height was

8 equal to tank diameter (H=T). Distilled water with a viscosity of 0.001 kg/ms, density of 998.00

9 kg/m^3 and interfacial tension of 71.90 mN.m^{-1} was used. The temperature of the water was

10 controlled and all the measurements were carried out at the room temperature (24 ^{o}C).

11 **Fig. 1.** Experimental setup: A; Motor, B; Shaft, C; Impeller, D; Tank, E: Speed analyzer, F;
12 Power analyzer, G1 and G2; Conductivity probes, H; Conductivity meter controller, I; Data
13 logger, J;   Computer, K; Injection point

14 **Fig. 2.** The used impellers in experimental part: (a) RT, (b) CB, (C) PBTU, (d) PBTD, (e) EB, (f)
15 PB, (g) HE3, (h) DCB [35]

16 **2.2   Determination of power consumption and power number (N_P)**

17 The power consumption and power number values for all of the impellers were obtained at

18 turbulent Reynolds number. It was measured directly from the motor using the power analyzer,

19 to compare the efficiency of different impeller design:

20 $$N_P = \frac{P}{\rho N^3 D^5}$$ (9)

21 Where "P" is Power required by the impeller, kg m^2/s^3; "N" is impeller rotational speed, rev/s,

22 "ρ" is liquid density, kg/m^3 and "D" is impeller diameter, m.

1   The power consumption is extremely dependent on Reynolds number [1, 36, 37]. Reynolds

2   number (N_{Re}) is demonstrated in equation 10 which reveals the ratio of inertial forces to viscous

3   forces.

4    $$N_{Re} = \frac{\rho N D^2}{\mu}$$ (10)

5   Where "μ" is the liquid viscosity, kg/s m.

6   The mean energy dissipation rate can be obtained through the following expression [11]:

7    $$\bar{\varepsilon} = \frac{P}{V_T \rho} = \frac{N_p N^3 D^5}{V_T}$$ (11)

8   Where "V_T' is the tank volume, m^3.

9   **2.3   The point of air entrainment**

10   The impeller speed at which air is entered from the surface of a stirred vessel for the first

11   time, is the air entrainment point N_E. The air entrainment point is very important for several

12   applications. In some applications air entrainment is not desirable and then a large N_E is needed

13   whereas for the others air is needed for more efficient processes and therefore, a small N_E is

14   desirable [38]. Air entrainment is taken place by interaction between the interfacial tensions and

15   the turbulent eddies at the surface of stirred vessel [39]. The N_E characteristics let to perform a

16   comparison on the amount of turbulence at the tank surface between various impeller geometries.

17   In the current study, air entrainment point was determined by observation of the liquid surface as

18   the point bubbles were started to entrain.

19   **2.4   Determination of mixing time**

20   The mixing time is experimentally defined by measurement of the concentration of injected

21   tracer within the stirred vessel. The concentration in the mixing tank is changed by tracer

1   injection. Macromixing or bulk blending time is defined when the concentration at the measuring

2   points reach to 95% ΔC. The conductivity is the most common method to measure the mixing

3   time. Therefore, it was applied to measure the mixing time in the current study. In this method,

4   an electrolyte is added through the vessel as a tracer to monitor the local conductivity against the

5   time. Solution of NaCl is used as an electrolyte commonly. 10 mL of NaCl Solution (250g/L)

6   was injected to the tank through the liquid surface, 30 mm from the wall through a syringe [1,

7   10, 19]. Two conductivity Suntex, EC.430 probes (Taiwan) with the accuracy of ±1% were fitted

8   to the wall; one was located at the opposite position of the injection point 80 mm lower than the

9   liquid surface and the other one was 80 mm over the bottom.

10   The conductivity outputs are used to evaluate the mixing time [40]. The time elapsed

11   between the injection of tracer and the point when the instant conductivity attained within 95%

12   of its final value is considered as the mixing time for each probe [1].

13    $$Y = \left| \frac{C(t) - C_0}{C_\infty - C_0} \right|$$ (12)

14   Where "$C_{(t)}$" is the concentration of the trace at time (t), "C_0" is the initial and "C_∞" is the final

15   average concentrations of tracer. Each test is repeated 3 times to get an average of the mixing

16   time.

17   The mixing efficiency (η) of the system can be obtained through the calculation of mixing

18   time (t_m) and mean specific energy dissipation rate ($\bar{\varepsilon}$) through the following expression [11]:

19    $$\eta = \bar{\varepsilon} t_m$$ (13)

1 ## 2.5   Mixing time prediction

2 ### 2.5.1   Non-linear regression method

3 Mixing time and power consumption were obtained for each impeller at three different off-

4 bottom clearances (T/3, T/4 and T/6) and a range of speed from 1.67 rps to 15 rps. The general

5 form of the relation between the mixing times, energy dissipation rate and impeller clearance in

6 single phase liquid system was derived from the literature as follows [5, 24, 25];

7 $$t_m = \alpha \left(\bar{\varepsilon} \right)^{\beta} \left(\frac{C}{T} \right)^{\gamma} \tag{14}$$

8 The experimental data were then fitted to the previously mentioned mixing time model to

9 determine the corresponding model parameters for each impeller. The transformation of

10 nonlinear equations into linear forms is generally associated with the error distribution,

11 depending on the method used to linearize the equations [41, 42]. Therefore, in this study, a non-

12 linear regression analysis using the Marquardt–Levenberg algorithm was employed in SigmaPlot

13 software version 12.0 (Systat Software Inc., USA) to determine the parameters associated with

14 the clearance and energy dissipation rate variables in the mixing time correlation. The nonlinear

15 coefficient of determination (R^2), was evaluated to quantitatively compare the goodness of fit of

16 the abovementioned model (Eq. 14) to the experimental data and adjust each set of mixing time

17 model parameters. The coefficient of strength of character, which determines how well the data

18 points fit the model, was calculated as follows [43];

19 $$R^2 = 1 - \left(\frac{\sum_{i=1}^{n} (t_{m(meas)} - t_{m(cal)})^2}{\sum_{i=1}^{n} (t_{m(meas)} - \overline{t_{m(meas)}})^2} \right) \cdot \left(\frac{n-1}{n-p} \right) \tag{15}$$

20 Where $\overline{t_{m(meas)}}$ is the experimental data average value; and "*p*" is the number of model

21 parameters.

12

2.5.2   ANFIS-Fuzzy C-Means

A fuzzy inference system may be employed towards mimicking specific features of human supervisory know-how to complete duties and avoiding to use comprehensive mathematical calculations. Neural networks (NNs) are in fact mathematical models to process data which are inspired by how a brain works. NNs, similar to the brain neurons, contain various interconnected computing cells. The training process of NNs ascertain a relationship is constructed between the input and output data [44]. Amalgamation of fuzzy logic (FL) with NNs has demonstrated potential of these structures in basically imitating the actual sequence of decision-making that a professional follows in comparable situations. The weight values of the interconnections varies throughout the training phase of the traditional NNs, however, in the hybrid designs of the FL and NNs, the learning capability of NN and the inference mechanism of the FL is combined towards a unified neuro-fuzzy supervisory system [45].

A neural network structure which comprises of numerous coupled nodes through indicator associations is an adaptive network. Each node is described by a node function with constant or variable parameters. In order to reduce the error, NN algorithms are utilized to discover the undetermined preliminary and succeeding rule parameters of the FL. The full details of the ANFIS method is given by Jang et al. [46].

In addition, in this work, Fuzzy C-means (FcM) is applied. FcM, introduced by Bezdek [47], is a data clustering method which permits one data portion to correspond to two or more clusters. Deciding on the how to categorize data from dataset in order to give a brief image of a system's performance is the objective of data clustering [47]. FcM distributes a set of n vector X_i, $i = 1, 2, \ldots, n$, into C fuzzy groups and identifies a cluster center in each one while minimizing a difference measure cost function.

1   The FcM algorithm steps can concisely be described as follows. Initially, the cluster centers

2   c_i, $i = 1, 2, \ldots, C$ are chosen arbitrarily from the n points $\{X_1, X_2, X_3, \ldots, X_n\}$. Then, the

3   membership matrix U is computed using the following equation:

4
$$\mu_{ij} = \frac{1}{\sum\limits_{k=1}^{c} \left(\dfrac{d_{ij}}{d_k} \right)^{\frac{2}{m-1}}} \tag{16}$$

5   Where, $d_{ij} = \left\| c_i - x_j \right\|$ is the Euclidean distance between the ith cluster center and j^{th} data point,

6   and m is the fuzziness index. Next, the cost function according to the following equation is

7   computed. The process is stopped if it is below a certain threshold.

8
$$J(U, c_1, \ldots, c_2) = \sum_{i=1}^{c} J_i = \sum_{i=1}^{c} \cdot \sum_{j=1}^{n} \mu_{ij}^m d_{ij}^2 \tag{17}$$

9   In the final step, a new c fuzzy cluster centers c_i, $i = 1, 2, \ldots, C$ using the following equation is

10   computed:

11
$$c_i = \frac{\sum\limits_{j=1}^{n} \mu_{ij}^m x_j}{\sum\limits_{j=1}^{n} \mu_{ij}^m} \tag{18}$$

12   By using a part of the experimental data and FcM-based ANFIS approach, the model showed to

13   be able to anticipate the mixing time. The target parameter in the model was the mixing time

14   while the tank clearance and the mean energy dissipation rate were chosen as the design

15   parameters. In order to develop the model, the experimental data points were separated into 70%,

16   15% and 15% segments for training, validation and test respectively. Table 1 encapsulates the

17   specifications of the designed ANFIS-FcM model.

18   **Table 1.** Specifications of the developed ANFIS-FcM model for mixing time prediction

3   Results and Discussion

3.1   The effect of impeller design on power number

The power number of each impeller was determined through direct measurement of the required power, P, to drive the impeller. The accuracy of the measurement method was verified by comparing the power number values for commonly used impellers with the literature. The variations of power number with Reynolds number for given impellers in this work at C=T/3 are illustrated in Fig. 3. All the experiments were carried out in a Reynolds number range of 5.0×10^4 to 15.0×10^4. The results showed that at the same geometry and agitation speed, the power number (N_P) for the hydrofoil impeller (HE3) at C=T/3 was 0.36 whereas for PBTD, PBTU, PB, EB and CB were 1.19, 1.75, 2.28, 2.96 and 3.25, respectively. The DCB and RT are ranked last with the values of 6.76 and 5.55. The results proved the power number of DCB and RT are almost 10 times than that of the hydrofoil impeller. The results indicated that the axial flow impellers and specifically the down-flow impellers have the lowest power number values among the impellers. The results clearly showed a reduction in the power number values for the radial flow impellers as the blade curvature increases. Moreover, the disk turbines have higher power number values than the impellers without central disk. The experiments indicate that for a given impellers, the power number did not vary in a turbulent regime, significantly. However, slight changes can be seen due to instability of the measurement device. The flow pattern has a significant role on power consumption and any changes on flow direction affect the power number value [48]. A tendency of the bubbles to accumulate at the low-pressure area leads to extend the gas cavity effect and conducts in a higher power values under un-aerated condition [49]. The high volume of air bubbles around the impeller region for the radial flow impellers

1   such as RT and DCB leads to an increase in the cavity effect and higher power consumption at

2   higher Reynolds numbers.Therefore, any parameter that makes an alteration in the flow or

3   turbulence, changes the power consumption.

4   **Fig. 3.** Comparison of N_P values for DCB (○), RT (♦), CB (■), EB (Δ), PB (●), PBTU (◊), PBTD

5   (▲) and HE3 (□) at C/T=1/3

6   **3.2   The effect of impeller off-bottom clearance on power**

7   The effect of clearance on impeller power consumption at three common clearance levels

8   including 1/3T, 1/4/T and 1/6T were tested. Furthermore, the effect of clearance on mean energy

9   dissipation rate for all impellers at different agitation speed, from 1.67 to 8.33 rps, were

10   examined and plotted. Fig. 4 illustrates a typical impellers trend at 5 rps. In case of disk turbines,

11   the value of impeller power number decreased with reduction in the clearance level from T/3 to

12   T/6. The disc causes higher kinetic energy in the entrained flow at a clearance of T/3 compared

13   with the lower clearance. The turbulent energy dissipation rate increases with an increase in the

14   path length in a turbulent flow, which improves the impeller pumping and reduction in the power

15   consumption [48]. For the RT, CB, EB, PBTU and PB a decrease in the off-bottom clearance

16   from T/3 to T/6 led to lower power number value whereas an increase was observed in the power

17   number values for PBTD and HE3. Also, a decrease in the clearance level led to shorter loops for

18   return flows in the up-flow turbines. Therefore, the flow has a higher energy which leads to

19   better impeller pumping and further reduction in impeller power number. Rewatkar and Joshi

20   [5], Rao and Joshi [14], Rewatkar et al. [48] and Zhao et al. [50] also reported the same trends

21   for PBTD and PBTU with decreasing clearance level. The reduction in clearance leads to an

22   increase in cross flows below the impeller area and higher velocity rate. In lower clearances, the

23   impeller output flow hits the tank bottom and changes the flow direction significantly,

1 consequently leading to higher energy dissipation rate and higher power number in down flow

2 impellers. The results for the DCB impeller at different clearance levels showed a significant

3 reduction in power number at level T/6 while for HE3 were mostly the same at different

4 clearances.

5 **Fig. 4.** The effect of clearance on power number in various impellers; (a) RT, (b) CB, (C) PBTU,

6 (d) PBTD, (e) EB, (f) PB, (g) HE3, (h) DCB

7 The mean energy dissipation rate, $\bar{\varepsilon}$, for the CB and EB configurations were 42% and 29%

8 larger than the PB at T=1/3 and 5 rps. The mean specific energies for the PBTU were 42%, 28%

9 and 3% larger than the PBTD at T/3, T/4 and T/6, respectively. However, the lowest values were

10 found for the HE3 among the studied impellers.

11 **3.3 The effect of impeller design and clearance on Air entrainment speed**

12 The influence of impeller design and clearance on N_E is illustrated in Fig. 5(a) for all the

13 studied impellers except for the HE3. Although, the test continued up to the speed of 20 rps for

14 the HE3 impeller, no any bubble was observed within the tank. The point of air entrainment N_E

15 is influenced by both the impeller type and the impeller clearance. The axial flow impellers

16 mostly can be used for higher agitation speed. The surface aeration was observed after 16 rps for

17 the Hydrofoil impeller, and for the PBTU and PBTD after 11.6 and 7 rps, respectively. For the

18 radial flow impellers, the highest air entrainment speed was observed for the EB after 7.5 rps.

19 The N_E values were observed in a range of 5 to 7 rps. The flow stream moves in two separate

20 loops from the walls towards the shaft near the liquid surface for the radial flow impellers. The

21 loops are created around the impeller blades in lower speed while they increase toward the tank

22 wall and top surface, causing the sucking of air bubbles inside the liquid wall [51]. In the case of

1   axial flow impellers, the flow for the down flow impeller (PBTD) is created one loop toward

2   shaft near the liquid surface and discharges the flow in the downward direction. However, for the

3   up-flow impellers, PBTU and HE3, the flow is pumped upward along the shaft toward the

4   surface and then circulates along the tank wall. This flow then loses its intensity and changes to a

5   weak flow below the impeller. In the down flow impellers, the gas bubbles are drawn down into

6   the central section of the tank and then distributed radially toward the tank wall and surface [51].

7   Therefore, air entrainment for radial flow impellers and PBTD is different compared to PBTU

8   and HE3 [52].

9   Bhattacharya et al. [38] reported that increasing the submergence caused a higher N_E which

10   was in a good agreement with our obtained results. Decreasing the impeller clearance reduced

11   the turbulent energy reaching the surface, resulting in a higher agitation speed to make bubbles at

12   the liquid surface. In the present study, this trend was observed for all the given impellers except

13   for the PBTU. This can be attributed to its upward flow pattern which pumps flow stronger in

14   lower clearances. The DCB impeller has a smaller N_E and is less sensitive to clearance. For the

15   EB, CB and PB, the N_E shows a fairly similar values and trends. In the case of up-pumping

16   impellers, a stronger discharge flow into the surface is generated in comparison with the down

17   pumping impellers. Thus, the lower power consumption has been obtained at lower clearances

18   for pitched blade up-flow impeller. The high velocity under the down flow impellers causes the

19   fluid to move along the bottom and then the top of the tank. Because of low-pressure regions

20   behind the impellers, the fluid does not move in a direct path to the surface, resulting in poor

21   circulation and mixing in the top of the tank [53].

22   Fig. 5(b) represents the mean energy dissipation rate for the impellers at the air entrainment

23   point. As expected, the mean energy dissipation rate was increased with decreasing the clearance

level, except for the PBTU. Although, the results for the PBTU at T/3 were higher than the PBTD, with decreasing the clearance, PBTU showed lower energy dissipation rate than the other impellers.

For the application where air entrainment is desired, N_E is a proper parameter to make a comparison between the impellers. Therefore, the PBTD provides the best performance with the lowest N_E and power consumption.

Fig. 5. a) N_E in terms of the impeller clearance and agitation speed b) Mean energy dissipation rate at the point of N_E in terms of the impeller clearance

3.4 Mixing time

3.4.1 Effect of various impeller type on mixing time

The mixing times were obtained for impeller agitation speeds of 1.67 to 8.33 rps, corresponding to Reynolds numbers of 5.0×10^4 to 15.0×10^4 at clearance level of (T/3) for all the studied impellers. Due to high air entrainment within the tank, the experiments were stopped at 8.3 rps for all of the impellers, except for the DCB. For the DCB, the experiment was stopped at 6.6 rps because of high air entrainment within the tank above this speed. Fig. 6 illustrates the results for mixing time against Reynolds number. The measurements proved the close mixing time values after Re=6.7×10^4 for all axial and radial impellers except for the hydrofoil impeller. Similar observation was made by Biggs, [54] and Rewatkar and Joshi [5] and Fentiman et al. [55].

Fig. 6. Mixing time against Reynolds number for various impellers

1   The graph illustrates that the DCB turbine can reach the desired mixing point at lower

2   Reynolds numbers while the mixing time values for the Hydrofoil impeller were 2 to 4 times

3   higher than the other impellers within the selected range of Reynolds number.

4   The experiments were conducted at the same power consumption to find out the effect of

5   impeller design on the mixing time. Fig. 7 represents the comparison of the mixing time for each

6   impeller at the same power consumption per volume (P/V) at T/3. The figure indicates that the

7   highest mixing time values at the same power consumption were obtained for the radial flow

8   impellers while the lowest were found for the axial flow impellers. The results verified very

9   close values for the radial and axial flow impellers in a range of 10.0 to 12.3 (s) and 7.6 to 8.9

10   (s). The best performance was observed for the PBDT. Very close values were also obtained for

11   the elliptical blade and curved blade impellers at the same power consumptions. Shorter mixing

12   times were predicted for the higher discharge rate impellers because of faster circulation within

13   the tank. In the case of radial flow impellers, the mixing time values increased as the blade

14   becomes more curved and therefore, mixing time values for the elliptical and parabolic blade

15   turbines was higher in comparison with curved blade and Rushton turbine. Therefore, the

16   obtained results prove the effect of flow diagram in the tanks influence the mixing efficiency.

17   **Fig. 7.** Comparison of the mixing time for different impellers at the same power consumption

18   (P/V=160 W/m^3)

19   **3.4.2   Effect of Clearance on mixing time**

20   The effect of off-bottom clearance on mixing time in the mixing vessels was studied for

21   each type of impellers through the T/3 to T/6 at 5 rps. As seen Fig. 8, for the pitched blade down-

22   flow impeller and hydrofoil impeller, the value of mixing time increased with a decreasing

23   clearance from T/3 to T/6. However, for the other impellers, the mixing time was found to

decrease when the clearance was decreased from T/3 to T/6. The plot signified that the highest

mixing time value was obtained for the HE3. In contrast, the PBDT shows better performance

and it can be a good choice even in lower clearance due to the lower power consumption

compared with radial flow impellers. In the case of HE3 and PBTD, decreasing the clearance

from T/3 to T/6 caused the generation of smooth flow and lower circulation velocity, which

resulted in higher mixing time values. Decreasing the clearance for the PBTU leads to a larger

circulation velocity and a better suction through tank and a lower mixing time value [14].

Decreasing the mixing time values in radial flow impellers with decreased in the clearance level

can be described with a larger path length and flow rate in the area on the top of the impeller.

The suction is divided by the disk and causes larger circulation velocities through upper and

lower loops in the tank, resulting in smaller mixing times. Moreover, as the blade becomes more

curved the slope of stream becomes smaller and causes a weaker radial jet. This resulted in

higher mixing times in elliptical and parabolic blade turbines in comparison with curved blade

and Rushton turbine [50].

Fig. 8. The effect of impeller clearance on mixing time at 5 rps

3.4.3   Correlation study

3.4.3.1   Empirical Correlation

As previously stated, the mean energy dissipation rate and the off-bottom clearance are two

significant variables that affect the mixing time. Thus, in the modeling of the mixing time in the

current study we implemented an approach that considers the effect of variation in clearance as

well as the variation in the mean energy dissipation rate due to the speed variation. The main

distinguishing feature for choosing a suitable model arises from the accuracy as well as

simplicity of the equations. Therefore, equation 14 was derived as a general form of the relation

1   between the mixing times, energy dissipation rate and impeller clearance in single phase liquid

2   system from the literature. The experimental mixing time data were fitted to the abovementioned

3   mixing time model and the corresponding parameters for each impeller were then adjusted.

4   For each studied impeller, a non-linear regression method was employed to independently

5   define the parameters according to the Equation 14. Table 2 represents the optimal values of the

6   model parameters. As evident in this table, the model parameters for each impeller varied when

7   the off-bottom clearance and the energy dissipation rate were changed.

8   Furthermore, the nonlinear regression coefficient (R^2) were evaluated and tabulated in Table

9   2 to quantitatively compare the quality of this method. The calculated values of R^2 verify the

10 capability of the recommended model to fit the experimental mixing time data for various

11 impellers at different experimental conditions. Fig. 9 illustrates the quality of the fit of this model

12 to the experimental data for studied impellers. The surface attained from the global fitting of the

13 above-mentioned model to the experimental data verifies that the experimental data are described

14 well for all clearance levels and energy dissipation rates when the mixing time plotted in

15 proportion to the proposed model used.

16   **Table 2.** Calculated values of the model parameters and associated R^2 for each impeller

17   **Fig. 9.** Graphical representations of the fit of the experimental data to the developed mixing
18   time model for all studied impellers

19

20 3.4.3.2   ANFIS-FcM model

21   As mentioned before, ANFIS–FcM was utilized in this study to build a substitute prediction

22 model to predict the mixing times from experimental data. The codes were written in the

23 MATLAB environment and a loop was defined in order to repeat the model development if the

final $R^2 \leq 0.999$. A dataset including 120 points was engaged. The predicted values for the mixing times by the ANFIS–FcM model in comparison with the measured values of mixing times is presented in Fig. 10.

Fig. 10. Prediction capability of ANFIS-FcM model vs. experimental data for the whole dataset

Fig. 11 represents evaluation of the estimated values of mixing time by the ANFIS-FcM model and Non-linear regression models. The regression plot proves FcM capability over the non-linear regression model when the results are compared to the experimental data points.

Fig. 11. Cross plot of predictions of ANFIS-FcM model and Non-linear regression model

4 Mixing efficiency

The mixing efficiency (η) was evaluated with considering both mixing time and the mean energy dissipation rate on different clearance and agitation speeds. The mixing efficiency (η) for the single-phase system can be evaluated through the equation (13) which has been derived by Ochieng & Onyango [11].

Clearly, lower values of (η) verify better efficiency within the mixing tank. Fig. 12 shows the P/V and the mixing time against the mixing efficiency values (η) at the clearance of T/3. The graph shows that increasing the power consumption and mixing time lead to higher value for η. On the other hand, the efficient systems are considered to be those that can reach the desired level in lower mixing time and power consumption. Moreover, the same value of η for each impeller can be seen at the intersection point of the two trend lines. This point is therefore assumed to be an efficient point for each impeller. With this assumption, the efficient points were attained for the axial flow impellers and especially for the hydrofoil and pitched blade

down flow turbines. The lowest efficiencies were obtained for the RT, CB and DCB. The performance of elliptical and parabolic blade shape was nearly the same. The calculated results provide a good comparison in the form of mixing time and energy dissipation rate for industrial purposes. The results confirmed that the axial impellers like pitched blade impellers are more efficient in liquid mixing compared to the radial flow turbines. Furthermore, the hydrofoil impeller can be a good choice for the process which needs slow bulk motions such as water treatment plants.

Fig. 12. The efficiency of impellers values (η) against the P/V and the mixing time at the clearance of T/3

5   Conclusion

Dispersion characteristics of various impeller designs through different off-bottom clearance levels were investigated by power consumption, mixing time and air entrainment point. In addition to the experimental study, accurate models were developed to predict the mixing time using non-linear regression method and ANFIS–FcM method. Four common impeller types in addition to three rarely used were chosen. A new curved blade impeller design was also developed for further studies. All the experiments were carried out in single liquid phase system and varying Reynolds number and agitation speeds. Reduction in power consumption was observed for the radial flow impellers as the blade's curvature increased. The lowest power numbers were obtained for the down flow impellers like HE3 and PBTD. Decreasing the off-bottom clearance from T/3 to T/6 led to lower power numbers for the up-flow impellers, whereas an increase was observed for the downward flow impellers. The results for air entrainment speed (N_E) showed that the DCB and RT reach to N_E very fast. The mixing time values for the DCB were the smallest whereas PBTD, RT, PBTU, CB, EB, PB, and HE3 were ranked after it,

1 respectively. The results indicated that the efficiency of pitched blade turbines were better than

2 the other impellers. Investigation on the effect of clearance on the mixing time demonstrated an

3 increase in the mixing time with decrease the clearance from T/3 to T/6 for PBTD and HE3

4 whereas it was decreased for the other studied impellers. The obtained results provide a good

5 comparison in the form of mixing time and energy dissipation rate at different clearance levels

6 for industrial purposes. The results confirmed better efficiency for axial-flow impellers

7 especially for down-flow ones. The results of the correlation studies revealed more accurate

8 predictions through the Anfis-FcM model compared to the regression method.

14 **NOMENCLATURE**

A	Blade angle. *degree*
B	Baffle width, *m*
C	Impeller clearance, *m*
c	Dimensionless constants
C_0	The initial concentrations of tracer
$C_{(t)}$	The tracer concentration at time (t)
C_∞	The final average concentrations of tracer
c_i	The d-dimension center of the cluster
D	Impeller diameter, *m*
d_{ij}	Euclidean distance between the ith cluster center and j^{th} data point
H	Tank Height, *m*
J_i	The ith of d-dimensional measured data
m	Fuzziness index (any real number greater than 1)
N	Agitation speed, *rps*

N_p	Impeller power number. dimensionless
N_{Re}	Reynolds number, dimensionless
n_b	Number of blades
n	Number of data points
P	Power consumption, $kg\ m^2/s^3$
p	Number of model parameters
R^2	Coefficient of determination
T	Tank diameter, m
t_m	Mixing time, s
$\overline{t_{m(meas)}}$	Average value of the experimental data, s
$t_{m(cal)}$	Calculated value of the mixing time, s
V_T	Tank volume, m^3
W	Blade Width, m
x_i	The ith of d-dimensional measured data
x_j	The ith of d-dimensional measured data

Greek Letters

ρ	Fluid density, $kg/\ m^3$
μ	Fluid viscosity, $kg/m\ s$
μ_{ij}	Membership matrix
η	Mixing efficiency
$\overline{\varepsilon_T}$	Mean energy dissipation rate, m^2/s^3

Subscripts

i	Cluster center
j	Data point
k	Iteration step

1

2 **References**

3 [1] I. Houcine, E. Plasari, R. David, Effects of the Stirred Tank's Design on Power Consumption
4 and Mixing Time in Liquid Phase, Chem. Eng. Technol. 23 (2000) 605-613.

5

6 [2] N.K. Nere, A.W. Patwardhan, J.B. Joshi, Liquid-Phase Mixing in Stirred Vessels: Turbulent
7 Flow Regime, Ind. Eng. Chem. Res. 42 (2003) 2661-2698.

8

9 [3] R. Afshar Ghotli, A.A.A. Raman, S. Ibrahim, S. Baroutian, Liquid-liquid mixing in stirred
10 vessels; A review, Chem. Eng. Commun. 200 (2013) 595-627.

11

12 [4] H. Kramers, G.M. Baars, W.H. Knoll, A comparative study on the rate of mixing in stirred
13 tanks, Chem. Eng. Sci. 2 (1953) 35-42.

[5] V.B. Rewatkar, J.B. Joshi, Effect of impeller design on liquid phase mixing in mechanically agitated reactors, Chem. Eng. Commun. 102 (1991) 1-33.

[6] J. Szoplik, J. Karcz, An Efficiency of the Liquid Homogenization in Agitated Vessels Equipped with Off-Centred Impeller, Chem. Pap 59 (2005) 373-379.

[7] T. Kumaresan, J.B. Joshi, Effect of impeller design on the flow pattern and mixing in stirred tanks, Chem. Eng. J. 115 (2006) 173-193.

[8] T. Kumaresan, N.K. Nere, J.B. Joshi, Effect of Internals on the Flow Pattern and Mixing in Stirred Tanks, Ind. Eng. Chem. Res. 44 (2005) 9951-9961.

[9] S. Masiuk, R. Rakoczy, Power consumption, mixing time, heat and mass transfer measurements for liquid vessels that are mixed using reciprocating multiplates agitators, Chem. Eng. Process. 46 (2007) 89-98.

[10] Y. Zhao, X. Li, J. Cheng, C. Yang, Z.-S. Mao, Experimental Study on Liquid-Liquid Macromixing in a Stirred Tank, Ind. Eng. Chem. Res. 50 (2011) 5952-5958.

[11] A. Ochieng, M.S. Onyango, Homogenization energy in a stirred tank, Chem. Eng. Process. 47 (2008) 1853-1860.

[12] A. Ochieng, M.S. Onyango, A. Kumar, K. Kiriamiti, P. Musonge, Mixing in a tank stirred by a Rushton turbine at a low clearance, Chem. Eng. Process. 47 (2008) 842-851.

[13] J.G. van de Vusse, Mixing by agitation of miscible liquids Part I, Chem. Eng. Sci. 4 (1955) 178-200.

[14] K.S.M.S. Raghav Rao, J.B. Joshi, Liquid phase mixing in mechanically agitated vessels, Chem. Eng. Commun. 74 (1988) 1-25.

[15] E. Rzyski, Liquid homogenization in agitated tanks, Chem. Eng.Technol. 16 (1993) 229-233.

[16] S.A. Ruszkowski, Rational Method for Measuring Blending Performance and Comparison of Different Impeller Types, Proc. Eighth Eur. Conf. Mixing, 1994, pp. 283.

[17] M.F.W. Distelhoff, A.J. Marquis, J.M. Nouri, J.H. Whitelaw, Scalar mixing measurements in batch operated stirred tanks, Can. J. Chem. Eng. 75 (1997) 641-652.

[18] J. Aubin, S. Kresta, J. Bertrand, C. Xuereb, D. Fletcher, Alternate operating methods for improving the performance of a continuous stirred tank reactor, Chem. Eng. Res. Des. 8 (2006) 569-582.

[19] S. Woziwodzki, Unsteady Mixing Characteristics in a Vessel with Forward-Reverse Rotating Impeller, Chem. Eng.Technol. 34 (2011) 767-774.

[20] R. Afshar Ghotli, A.R. Abdul Aziz, S. Ibrahim, S. Baroutian, A. Arami-Niya, Study of various curved-blade impeller geometries on power consumption in stirred vessel using response surface methodology, J. Taiwan Ins. Chem. Eng. 44 (2013) 192-201.

[21] Y. Sano, H. Usui, Interrelations among mixing time, power number, and discharge flow rate number in baffled mixing vessels., J. Chem. Eng. Jpn. 18 (1985) 47-52.

[22] Procházka J., Landau J., Homogenization of miscible liquids by rotary impellers, Collect. Czech. Chem. Commun. 26 (1961) 2961-2974.

[23] A.K. Coker, Fluid Mixing in Reactors, Modeling of Chemical Kinetics and Reactor Design, Gulf Professional Publishing, Woburn, 2001, 552-662.

[24] M. Moo-Young, K. Tichar, F.A.L. Dullien, The blending efficiencies of some impellers in batch mixing, AIChE J. 18 (1972) 178-182.

[25] A.W. Nienow, On impeller circulation and mixing effectiveness in the turbulent flow regime, Chem. Eng. Sci. 52 (1997) 2557-2565.

[26] L. Pakzad, F. Ein-Mozaffari, S.R. Upreti, A. Lohi, Characterisation of the mixing of non-newtonian fluids with a scaba 6SRGT impeller through ert and CFD, Can. J. Chem. Eng. 91 (2013) 90-100.

[27] K. Van't Riet, J. Tramper, Basic Bioreactor Design, Marcel Dekker, New York, 1991.
[28] R.K. Grenville, S. Ruszkowski, E. Garred, Blending of miscible liquids in the turbulent and transional regimes, 15th NAMF Mixing Conference,Banff, Canada, 1995.

[29] R.K. Grenville, A.W. Nienow, Blending of Miscible Liquids, Handbook of Industrial Mixing, John Wiley & Sons, Inc.2004, pp. 507-542.

[30] V.C. Hass, A.W. Nienow, A new axial pumping agitator for the dispersion of gas in liquids, Chem. Ing. Technik 61 (1989) 152-154.

[31] F. Saito, A.W. Nienow, S. Chatwin, I.P.T. Moore, Power, gas dispersion and homogenisation characteristics of SCABA SRGT and Rushton turbine impellers., J. Chem. Eng. Jpn. 25 (1992) 281-287.

[32] J.A. Shaw, Understanding the effects of impeller type, diameter and power on mixing time, Chem. Engng Prog. (1994) 45-48.

[33] A.B. Pandit, J.B. Joshi, Mixing in Mechanically Agitated Gas-Liquid Contactors, Bubble Columns and Modified Bubble Columns, Chern. Eng. Sci. 38 (1983) 1189-1215.

[34] A.H.P. Skelland, L.T. Moeti, Effects of surface active agents on minimum impeller speeds for liquid-liquid dispersion in baffled vessels, Ind. Eng. Chem. Res. 28 (1989) 122-127.

[35] R. Afshar Ghotli, M.R. Abbasi, A. Bagheri, A.A.A. Raman, S. Ibrahim, H. Bostanci, Experimental and modeling evaluation of droplet size in immiscible liquid-liquid stirred vessel using various impeller designs, J. Taiwan Ins. Chem. Eng.100 (2019) 26-36.

[36] W. Bujalski, A.W. Nienow, S. Chatwin, M. Cooke, The dependency on scale of power numbers of Rushton disc turbines, Chem. Eng. Sci. 42 (1987) 317-326.

[37] J.P. Chen, F.B. Higgins, S.-Y. Chang, Y.-T. Hung, Mixing, Physicochemical Treatment Processes2005, pp. 47-101.

[38] M.B. Machado, J.R. Nunhez, D. Nobes, S.M. Kresta, Impeller characterization and selection: Balancing efficient hydrodynamics with process mixing requirements, AIChE J. 58 (2012) 2573-2588.

[39] S. Bhattacharya, D. Hebert, S.M. Kresta, Air Entrainment in Baffled Stirred Tanks, Chem. Eng. Res. Des. 85 (2007) 654-664.

[40] E.L. Paul, V.A. Atiemo-Obeng, S.M. Kresta, Handbook of industrial mixing, John Wiley & Sons, Inc.2004.

[41] M.S. Shafeeyan, W.M.A.W. Daud, A. Shamiri, N. Aghamohammadi, Adsorption equilibrium of carbon dioxide on ammonia-modified activated carbon, Chem. Eng. Res. Des. 104 (2015) 42-52.

[42] Y. S. Ho, J. F. Porter, G. McKay, Equilibrium Isotherm Studies for the Sorption of Divalent Metal Ions onto Peat: Copper, Nickel and Lead Single Component Systems, Water, Air, and Soil Poll. 141 (2002) 1-33.

[43] M.S. Shafeeyan, W.M.A. Wan Daud, A. Houshmand, A. Arami-Niya, The application of response surface methodology to optimize the amination of activated carbon for the preparation of carbon dioxide adsorbents, Fuel 94 (2012) 465-472.

[44] P. Khosropanah, A.R. Ramli, M.R. Abbasi, M.H. Marhaban, A. Ahmedov, A hybrid unsupervised approach toward EEG epileptic spikes detection, Neural Comput. Appl. 1 (2018).

[45] C.T. Lin, C.S.G. Lee, Neural-network-based fuzzy logic control and decision system, IEEE T. Comput. 40 (1991) 1320-1336.

[46] J.S.R. Jang, ANFIS: adaptive-network-based fuzzy inference system, IEEE T Syst Man Cy-S. 23 (1993) 665-685.

[47] J.C. Bezdek, Fuzzy mathematics in pattern classification, Cornell University1973.

[48] V.B. Rewatkar, K.S.M.S.R. Rao, J.B. Joshi, Power consumption in mechanically agitated contactors using pitched bladed turbine impellers., Chem. Eng. Commun. 88 (1990) 69 - 90.

[49] A.W. Nienow, Mixing studies: a comparison of Rushton turbine with some modern impellers, Chem. Eng. Res. Des. 74A (1996) 417-423.

[50] J. Zhao, Z. Gao, Y. Bao, Effects of the Blade Shape on the Trailing Vortices in Liquid Flow Generated by Disc Turbines, Chin. J. Chem. Eng.19 (2011) 232-242.

[51] N.A. Deshmukh, J.B. Joshi, Surface Aerators, Chem. Eng. Res. Des. 84 (2006) 977-992.

[52] R.G. Mali, A.W. Patwardhan, Characterization of onset of entrainment in stirred tanks, Chem. Eng. Res. Des. 87 (2009) 951-961.

[53] J. Aubin, P. Mavros, D.F. Fletcher, J. Bertrand, C. Xuereb, Effect of Axial Agitator Configuration (Up-Pumping, Down-Pumping, Reverse Rotation) on Flow Patterns Generated in Stirred Vessels, Chem. Eng. Res. Des. 79 (2001) 845-856.

[54] R.D. Biggs, Mixing rates in stirred tanks, AIChE Journal 9 (1963) 636-640.

[55] N.J. Fentiman, N. St.Hill, K.C. Lee, G.R. Paul, M. Yianneskis, A Novel Profiled Blade Impeller for Homogenization of Miscible Liquids in Stirred Vessels, Chem. Eng. Res. Des. 76 (1998) 835-842.

1
2
3
4
5
6
7
8
9
10
11
12
13
14
15
16
17
18
19
20
21
22
23
24
25

List of Figures

Fig. 1. Experimental setup: A; Motor, B; Shaft, C; Impeller, D; Tank, E: Speed analyzer, F; Power analyzer, G1 and G2; Conductivity probes, H; Conductivity meter controller, I; Data logger, J; Computer, K; Injection point

Fig. 2. The used impellers in experimental part: (a) RT, (b) CB, (C) PBTU, (d) PBTD, (e) EB, (f) PB, (g) HE3, (h) DCB [35]

Fig. 3. Comparison of N_P values for DCB ($\circ$), RT ($\blacklozenge$), CB ($\blacksquare$), EB (Δ), PB ($\bullet$), PBTU ($\lozenge$), PBTD ($\blacktriangle$) and HE3 ($\square$) at C/T=1/3

Fig. 4. The effect of clearance on power number in various impellers; (a) RT, (b) CB, (C) PBTU, (d) PBTD, (e) EB, (f) PB, (g) HE3, (h) DCB

Fig. 5. a) N_E in terms of the impeller clearance and agitation speed b) Mean energy dissipation rate at the point of N_E in terms of the impeller clearance

Fig. 6. Mixing time against Reynolds number for various impellers

Fig. 7. Comparison of the mixing time for different impellers at the same power consumption (P/V=160 W/m^3)

Fig. 8. The effect of impeller clearance on mixing time at 5 rps

Fig. 9. Graphical representations of the fit of the experimental data to the developed mixing time model for all studied impellers

Fig.10. Prediction capability of ANFIS-FcM model vs. experimental data for the whole dataset

Fig. 11. Cross plot of predictions of ANFIS-FcM model and Non-linear regression model

Fig. 12. The efficiency of impellers values (η) against the P/V and the mixing time at the clearance of T/3
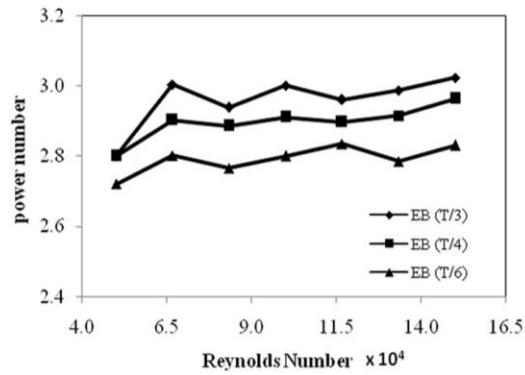
Fig. 1.

RT

CB

PBTU

PBTD

EB

PB

HE3

DCB
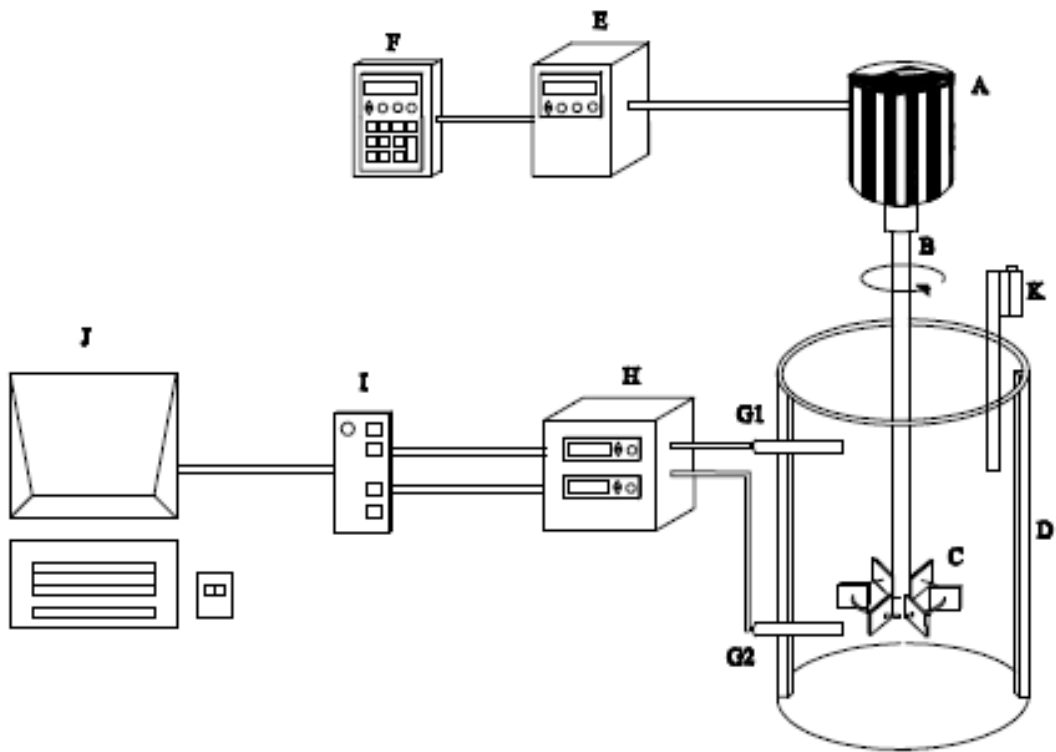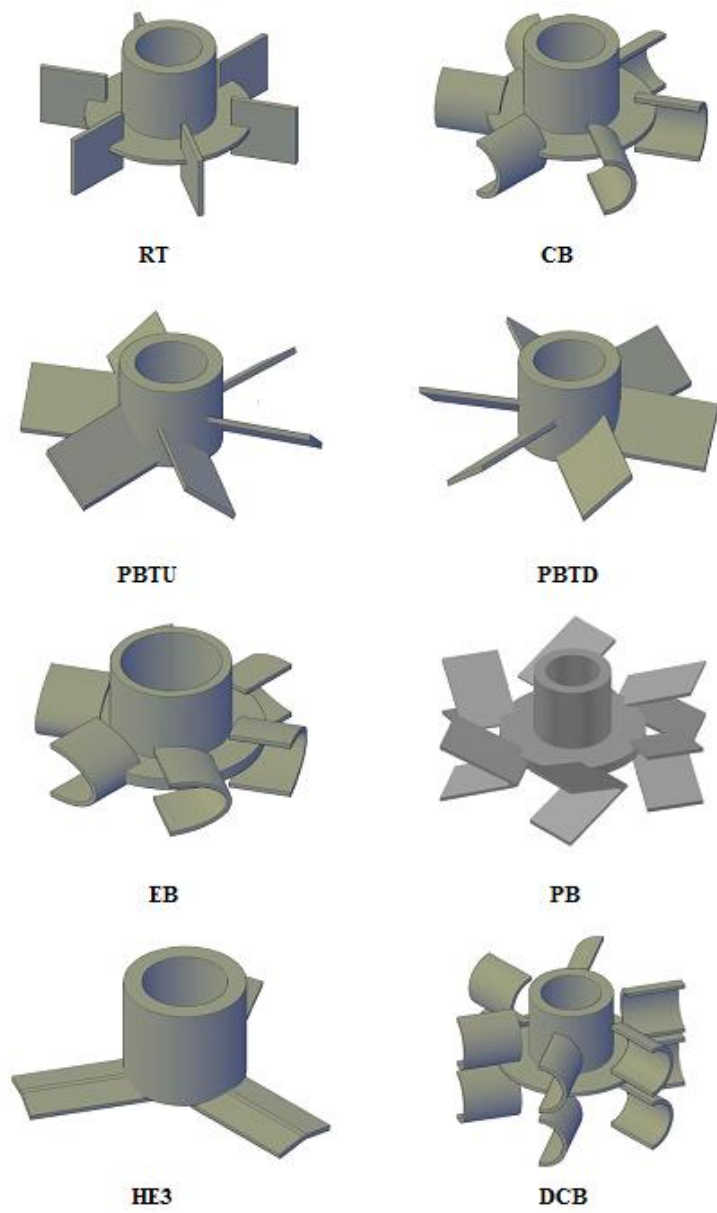
Fig. 2.
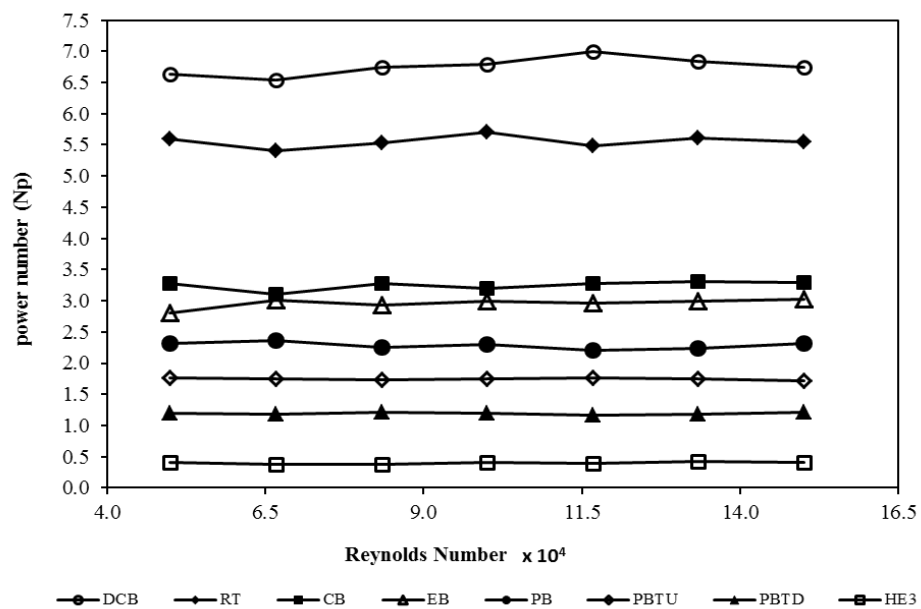
Fig. 3.

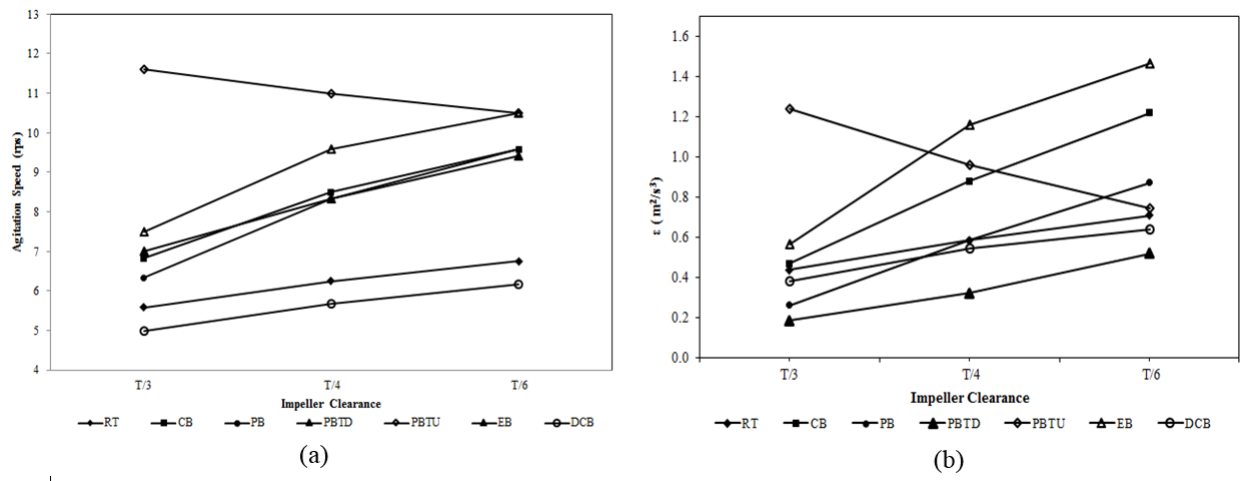(a) (b) (c) (d) (e) (f) (g) (h)

Fig. 4.

(a)   (b)
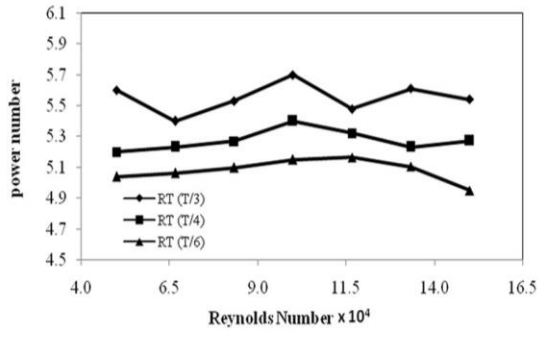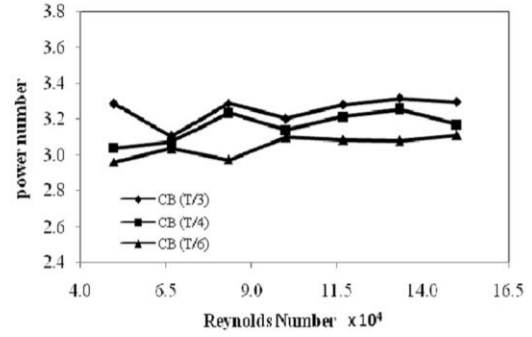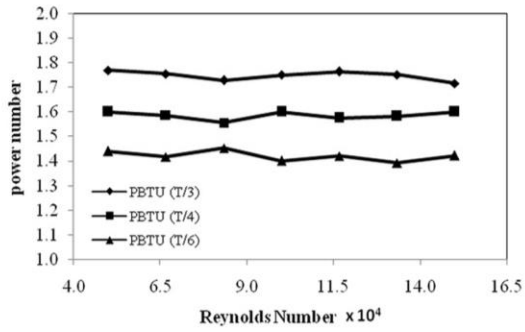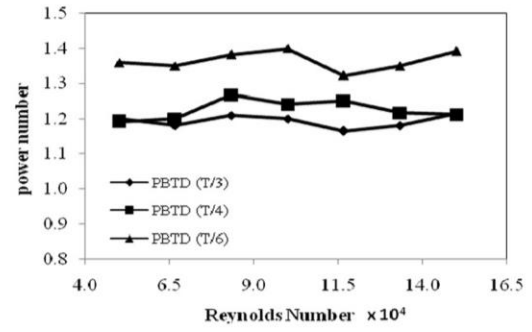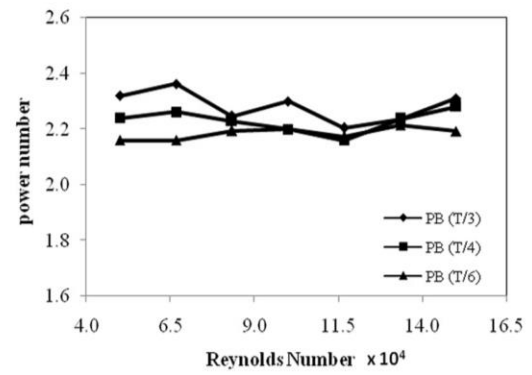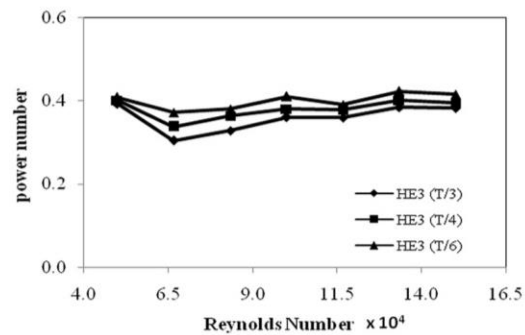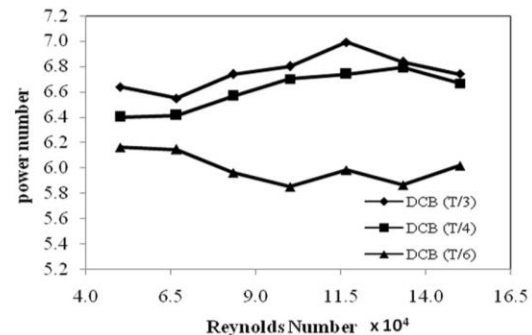
Fig. 5.
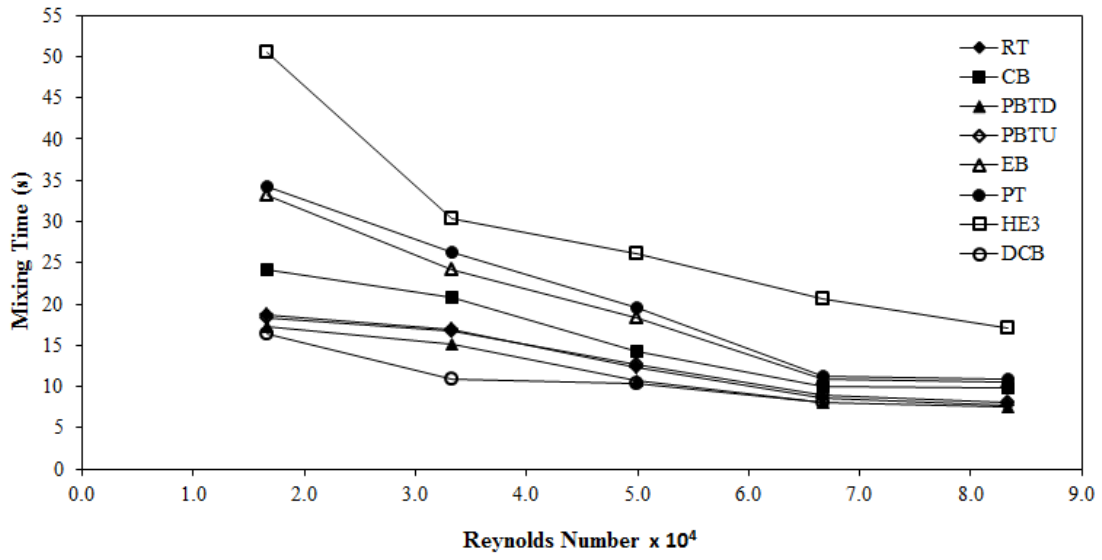
Fig. 6
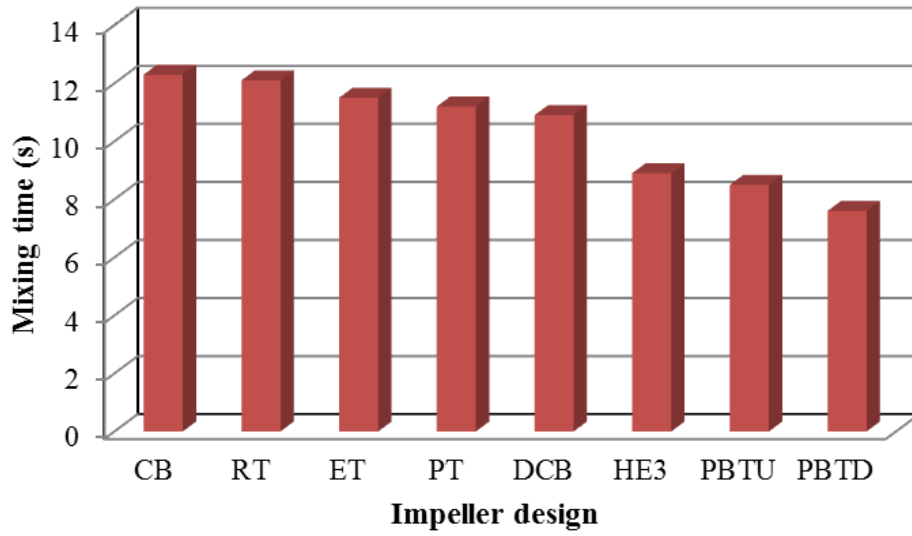
Fig. 7.
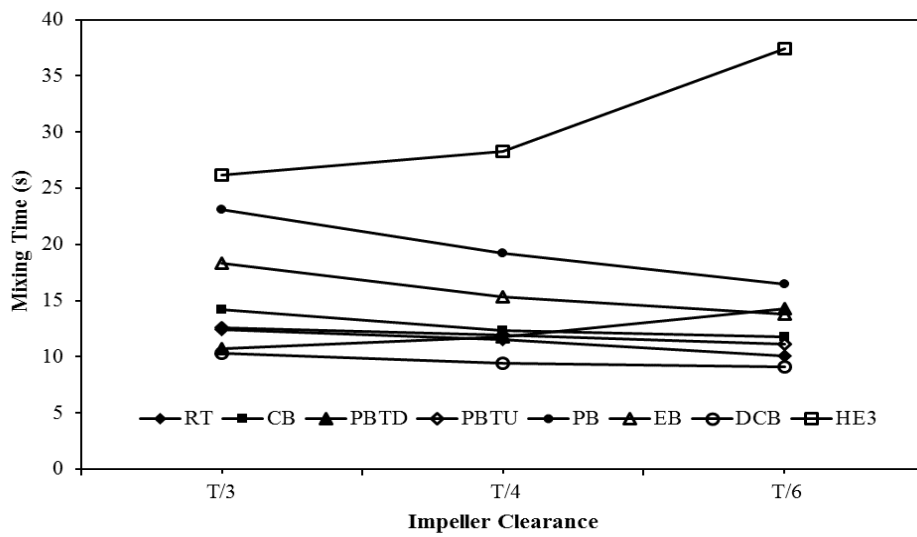
Fig. 8.
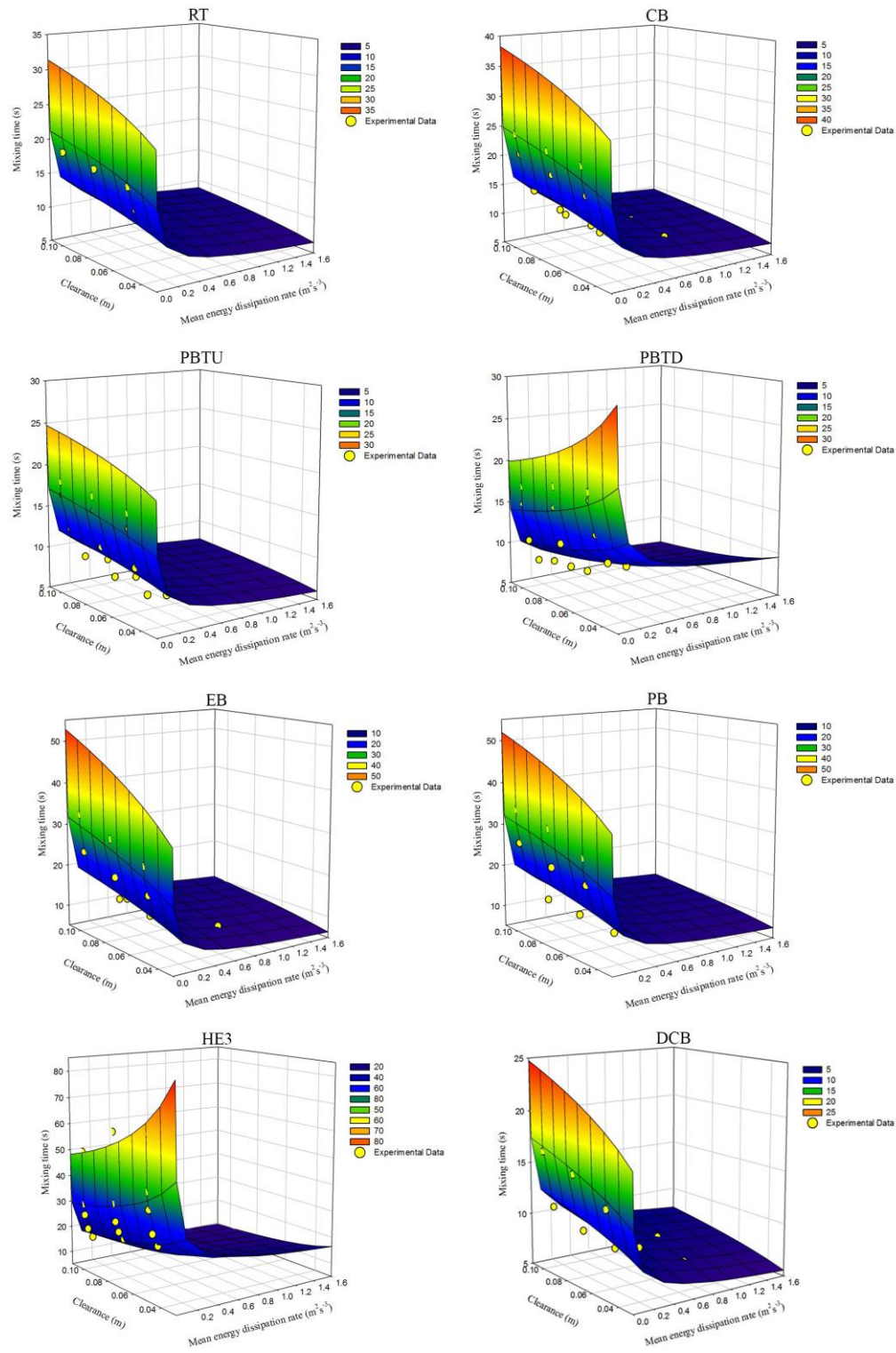
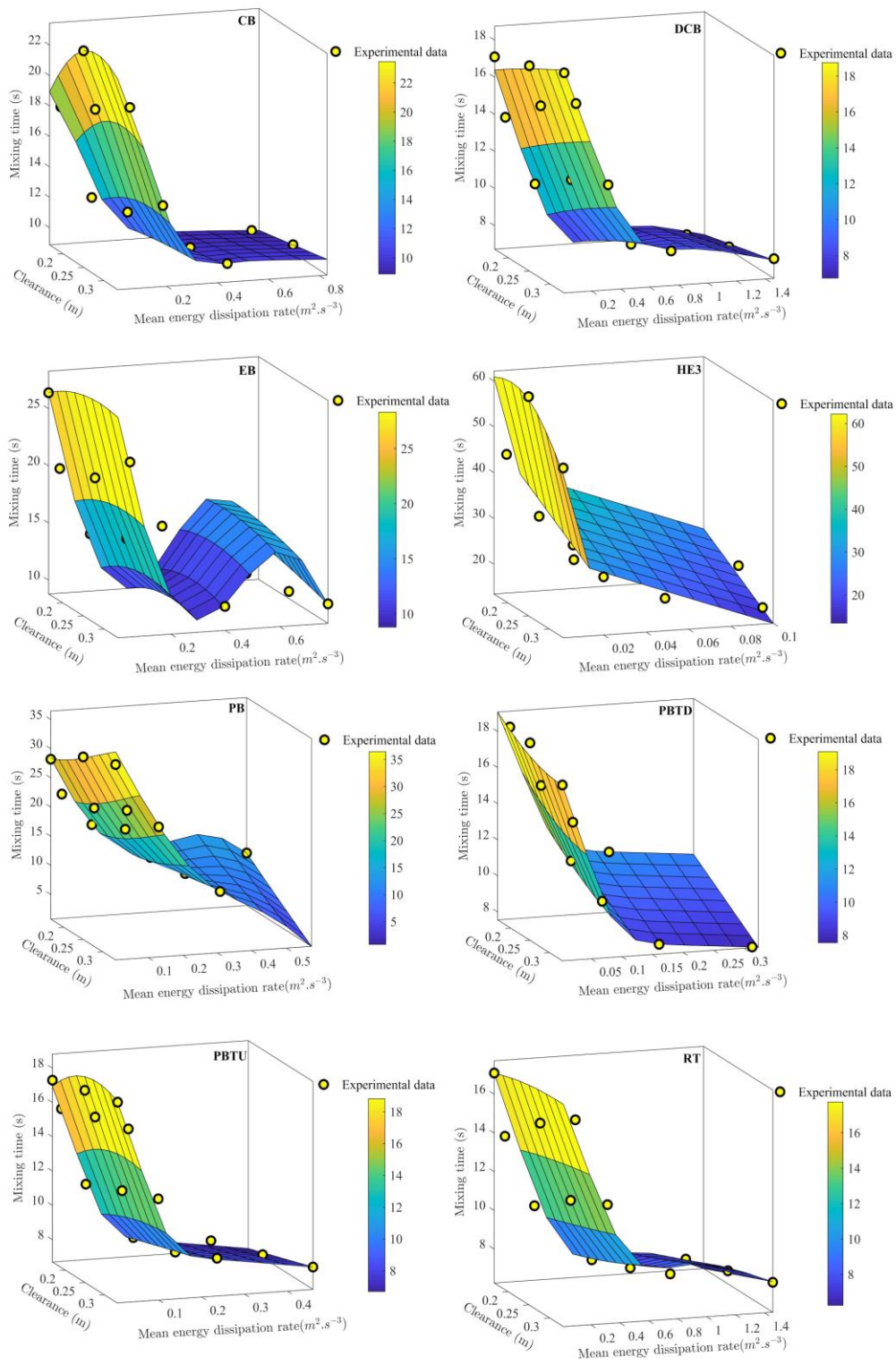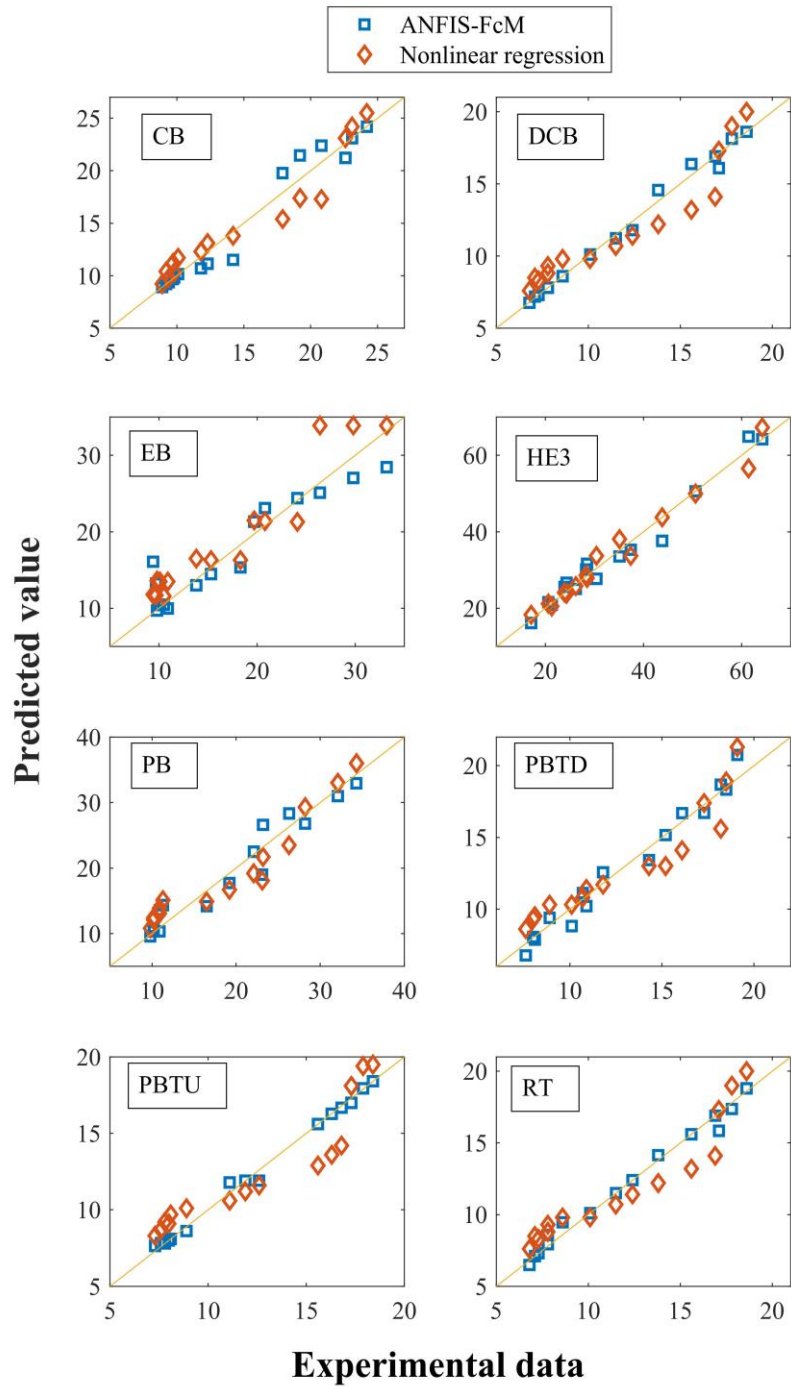**Fig. 9.**

Fig. 10.

Fig. 11.

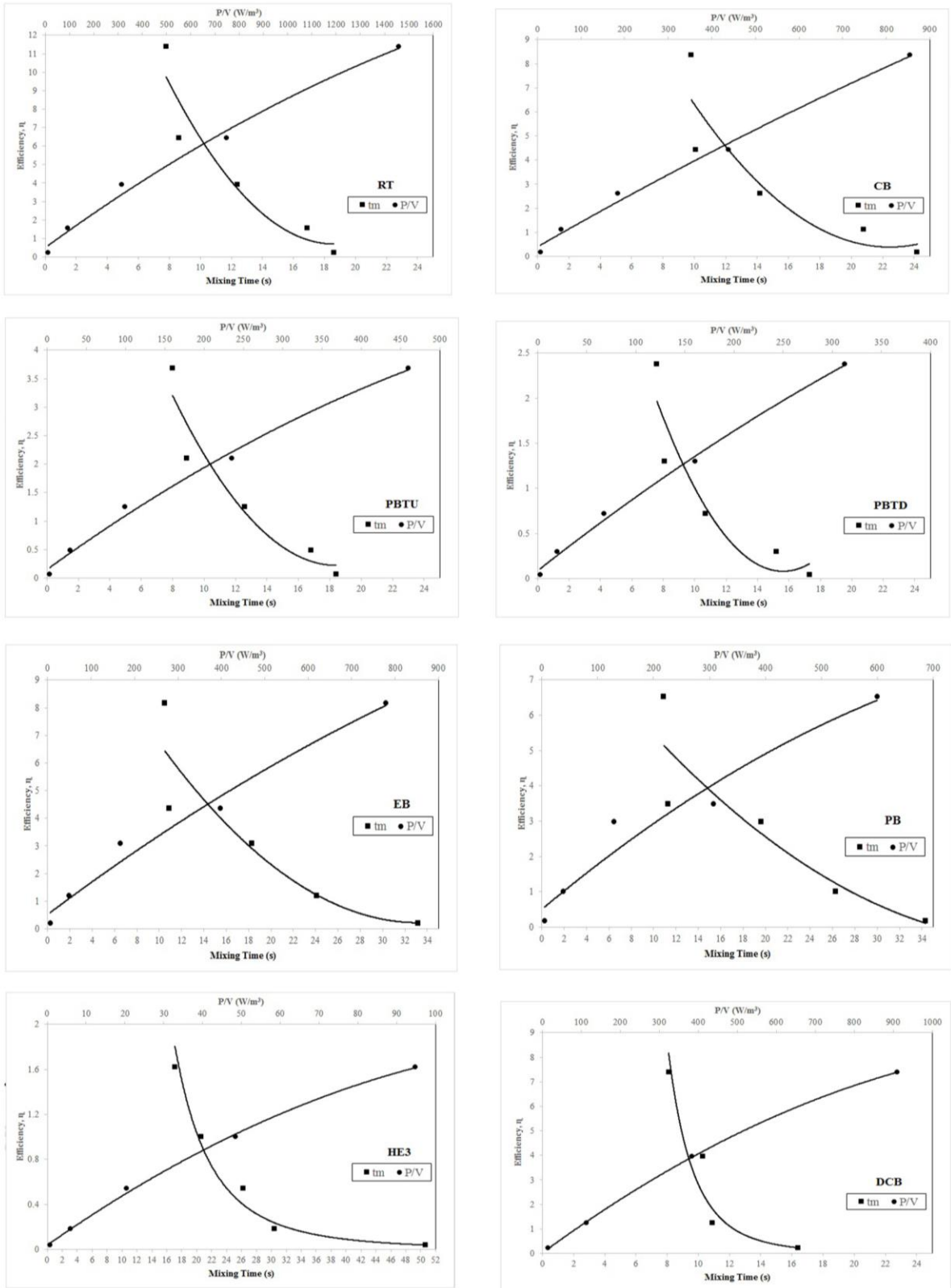**Fig. 12.**

List of Tables

Table 1.

Specifications of the developed ANFIS-FcM model for mixing time prediction

Parameter	Description
Number of nodes	17
Number of linear parameters	6
Number of nonlinear parameters	8
Total number of parameters	14
Number of training data pairs	7
Number of checking data pairs	4
Number of epochs	30
Fuzzy structure	Sugeno
Membership function type	Gaussian
Number of inputs	2
Number of outputs	1
Optimization method	Hybrid (least square and back propagation technique)
Number of fuzzy rules	2

Table 2.

Calculated values of the model parameters and associated R^2 for each impeller

Impeller Design	α	β	γ	R^2
RT	15.98	-0.172	0.233	0.891
CB	17.88	-0.189	0.247	0.934
PBTD	3.68	-0.151	-0.292	0.882
PBTU	11.99	-0.161	0.176	0.857
EB	25.83	-0.222	0.371	0.966
PB	23.21	-0.211	0.295	0.907
DCB	15.77	-0.154	0.278	0.961
HE3	4.061	-0.221	-0.429	0.977